JOURNAL OF NANO- AND ELECTRONIC PHYSICS
Vol. **11** No 2, 02025(5pp) (2019)

ЖУРНАЛ НАНО- ТА ЕЛЕКТРОННОЇ ФІЗИКИ
Том **11** № 2, 02025(5cc) (2019)

The Simultaneous Impacts of the *p nc*-SiO*x*:H Window Layer Band Gap and the Back Reflection on the Performances of a-Si:H Based Solar Cells

Abbas Belfar*, Mohammed Belmekki, Ferroudja Hammour, Hocine Ait-Kaci

Laboratory of Plasma Physics, Conductor Materials and their Applications, Faculty of Physics, Oran University of Sciences and Technology Mohamed Boudiaf USTO-MB, BP1505 Oran, Algeria

(Received 20 December 2018; revised manuscript received 08 April 2019; published online 15 April 2019)

In this study we have presented an investigation, by using numerical simulation, the simultaneous impacts of the *p nc*-SiO*x*:H window layer band gap (E_g) and the back reflection (RB) on the photovoltaic performances of hydrogenated amorphous silicon (a-Si:H) solar cells. For simulation, we have used the AMPS-1D (One Dimensional Analysis of Microelectronic and Photonic structures) code. The modeling was carried out on two configurations of the studied cell, one without rear reflector (RB = 0) and the other with rear reflector (RB = 0.8). The simulated results showed that the best output parameters of the cell were obtained in the case of the structure with rear reflector and when the value of the p-window layer band gap lies in the range from 2.05 eV to 2.10 eV. On the one hand, the values of the band diagram discontinuities on the conduction band levels ΔE_{C1} and ΔE_{C2} and on the valence band levels ΔE_{V1} (interface between the window layer and the buffer layer) and ΔE_{V2} (interface between the buffer layer and the active layer) are investigated to better understand the efficiency (E_{ff}) variations as a function of the window layer E_g. On the other hand, it is also obtained that the spectral response (SR) is very sensitive to the window layer band gap variations in the wavelength range from 0.35 to 0.55 μm for both cases. However, the spectral response decreases with the increase of E_g. Finally, the solar cell spectral response has improved in the wavelength range from 0.55 to 0.7 μm, and the best efficiency value (E_{ff} = 11.43 %) was obtained in the case of the structure with rear reflector.

Keywords: Solar cell, Hydrogenated nanocrystalline silicon oxide, Back reflection, Window layer band gap.

DOI: 10.21272/jnep.11(2).02025 PACS numbers: 73.40.Lq, 78.20.Bh

1. INTRODUCTION

Hydrogenated amorphous silicon (a-Si:H) is an attractive material for photovoltaic (PV) solar energy applications. Due to the nature of the thin film and the capacity of the large area substrates, the solar cell based on a-Si:H has been considered as one of the low-cost photovoltaic technologies. It has attracted many studies and continued a long and difficult road between initial laboratory study [1], industrial research and development production of PV modules [2-4]. Nevertheless, the low efficiency of the solar cell based on a-Si:H is mainly due to the poor transport of load carriers with a low mobility factor and lifetime ($\mu\tau$) [5, 6], in particular, for the holes. However, the efficiency of the stable cell reaches the maximum at a much thinner i layer than the initial efficiency, and then decreases with the thickness of the same layer because the light-induced generation of defects leads to a high recombination rate [7]. Optically, it is necessary to increase the thickness of the i layer for a sufficient absorption of the light to generate a high density photocurrent, but electrically it is necessary to keep the i layer thin enough to ensure a high internal electric field to collect the photogenerated carriers and to avoid a serious degradation of the efficiency induced by the light. Therefore, optimization of the efficiency of solar cells a-Si:H was confronted with a contradicted case. Therefore, to solve the optical and electrical contradictions, the use of a p-type window or buffer layer based on B-doped hydrogenated nanocrystalline silicon oxide (*p-nc*-SiO*x*:H) seems a good solution. The latter is characterized by a suitable refractive index and a wide band gap to reduce reflection in the front and minimize absorption in the *p*-layer, which is extremely important for ultra-thin solar cells [8].

The study carried out in this work was conducted on two solar cells of substrate type (*n-i-p*), one without rear reflector (RB = 0) and the other with rear reflector (RB = 0.8). The two cells are based on two materials, namely hydrogenated amorphous silicon (a-Si:H) and hydrogenated nanocrystalline silicon oxide (*nc*-SiO*x*:H). The simulation is focused on the investigation of the simultaneous effect of the *p nc*-SiO*x*:H window layer band gap (E_g) and the back reflection (RB) on the performances of the solar cell.

2. THE SIMULATED STRUCTURE AND SIMULATION MODEL

Our simulated solar cell is considered deposited on a metal substrate that plays the role of back contact. For the front contact, a TCO (Transparent Conducting Oxide) layer has been deposited on the p window layer side. The structure consists of an intrinsic a-Si:H layer with a thickness of 300 nm sandwiched between a n-Si:H layer with a thickness of 25 nm and a *p*-window layer based on hydrogenated nanocrystalline silicon oxide (*p-nc*-SiO*x*:H) with a thickness of 10 nm (Fig. 1).

A *p-nc*-SiO*x*:H buffer layer with a thickness of 5 nm was incorporated between the p-window layer and the *i*-a-Si:H active layer.

The AMPS-1D (One Dimensional Analysis of Microelectronic and Photonic structures) calculation code was used to simulate our solar cells. This software is

* abbasbelfar@gmail.com

based on the simultaneous resolution of the Poisson equation coupled to the continuity equations of electrons and holes at each position in the simulated structure. This resolution is performed by finite difference and Newton-Raphson methods.

This code simulates the operation of the device taking into account the Shockley-Read-Hall (SRH) recombination statistics. Numerical simulation also requires a model for the density of trapped states in the structure [9-12].

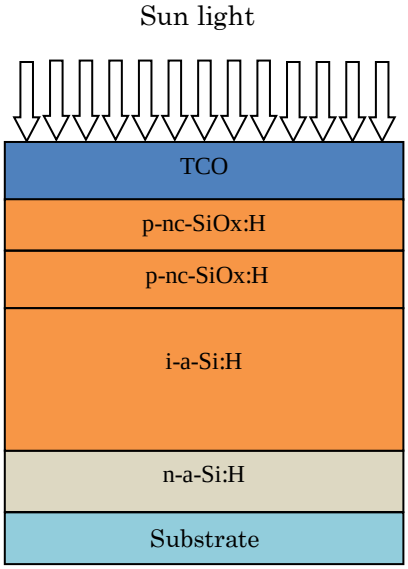

Fig. 1 – Schematic diagram of the simulated structure

For the local state density present in the gap of amorphous silicon and hydrogenated nanocrystalline silicon oxide, the AMPS-1D code assumes the existence of two types of states, the acceptor states and the donor states. Both these donor and acceptor-like states consisted of tail states and midgap defect states (dangling bonds). The tail states were approximated by the exponential distribution. Whereas the midgap defects were modeled using two Gaussian distributions and are usually given as follows:

$$g_{DG}(E) = \left(\frac{N_{DG}}{\sqrt{2\pi}\sigma_{DG}}\right) exp\left(-\frac{(E-E_{DG})^2}{2{\sigma_{DG}}^2}\right) \quad (1)$$

$$g_{AG}(E) = \left(\frac{N_{AG}}{\sqrt{2\pi}\sigma_{AG}}\right) exp\left(-\frac{(E-E_{AG})^2}{2{\sigma_{AG}}^2}\right) \quad (2)$$

In these equations, N_{DG} and N_{AG} are the total number of states in the Gaussian (cm^{-3}), E_{DG} and E_{AG} are the energy position (in eV) of the Gaussian peaks, and σ_{DG} and σ_{AG} are the standard energy deviations (also in eV). AMPS-1D assumes that midgap states can be modeled using a donor level to represent the D^+/D^0 dangling-bond configuration and an acceptor level to represent the D^0/D^- configuration [12, 13].

The AMPS-1D code requires two types of input parameters, electrical and optical.

Electrical input parameters

- Barrier height. The barrier heights of the front contact Φ_{bo} (TCO/p-window layer) and back contact Φ_{bL} (n layer/metal) were set at 1.45 eV and 0.2 eV, respectively.
- Electronic affinity (χ). χ is assumed to be different for hydrogenated nanocrystalline silicon oxide layers (*p-nc*-SiO*x*:H) and for layers based on hydrogenated amorphous silicon (a-Si:H).
- Surface recombination velocities. The surface recombination velocities of electrons and holes were both equal to $1 \cdot 10^7$ cm/s.
- Energies of the donor and acceptor states. For the *p-nc*-SiO_x:H layers, we used the values of 0.06 eV and 0.03 eV for the first *p* layer (window), and for the second p layer (buffer) the values of 0.05 eV and 0.02 eV were used as characteristic energies for the donor and the acceptor states, respectively.

All electrical parameters used in this simulation are shown in Table 1.

Optical input parameters

As a source of illumination, an AM 1.5 solar radiation with a power density of 100 mW/cm² was used. The light absorption coefficient, for the different layers was already incorporated in the AMPS-1D program.

For the light reflection, the value of 0.2 was chosen for the front contact. For the back contact, two values were used: RB = 0 for the structure without rear reflector and RB = 0.80 for the structure with rear reflector.

3. RESULTS AND DISCUSSION

Study of the cell performances as a function of the *p-nc*-SiO*x*:H window layer band gap and the back reflection

To investigate the effect of the *p-nc*-SiO*x*:H window layer band gap (E_g) on the performance of our solar cell described previously, we have varied the values of E_g between 1.90 eV and 2.25 eV. This simulation was conducted for two different values of the back reflection; RB = 0 (absence of a rear reflector) and RB = 0.8 (presence of a rear reflector).

The simulation results are shown in Fig. 2. In the latter we have illustrated the variations of the four cell output parameters, namely, the short-circuit current (J_{SC}), the open circuit voltage (V_{OC}), the fill factor (FF) and the conversion efficiency (E_{ff}).

It can be seen that the value of J_{SC} (Fig. 2a) decreases with the increase of the window layer band gap. However, the presence of the rear reflector (RB = 0.8) improves the value of the short-circuit current J_{SC}. This improvement of J_{SC} is obviously due to the presence of a rear reflector, which leads to the improvement of the spectral response (SR) presented in the Fig. 3. Knowing that, the expression of J_{SC} is given as follows:

$$\boldsymbol{J_{SC} = q\int_{(\lambda)} \Phi(\lambda)\{1 - R(\lambda)\}QE(\lambda)d\lambda} \quad (3)$$

where $QE(\lambda)$ is the quantum efficiency; $R(\lambda)$ is the reflection coefficient from the top surface; $\Phi(\lambda)$ is the photon flux incident on the solar cell at wavelength λ. The integration is carried out over the whole range of wavelengths λ of light absorbed by the structure.

From Fig. 3, we can see that the spectral response is less stable in the wavelength range of 0.35 μm up to 0.55 μm for both cases. It is also clear that in this wavelength range the spectral response is very sensitive to variations of the window layer band gap (E_g). However, the spectral response decreases with the increase of E_g. We can also see that the spectral response of the solar cell has improved in the wavelength range from 0.55 to 0.7 μm in the case of the structure with a rear reflector.

The open-circuit voltage (V_{OC}) variations are shown in Fig. 2b. In both cases, the value of V_{OC} increases from 0.905 V to 0.945 V when the value of E_g increases from 1.90 eV to 2.10 eV. Beyond 2.10 eV, the V_{OC} decreases gradually. However, the V_{OC} is very little affected by the presence or not of a rear reflector.

The fill factor (FF) presented in Fig. 2c is also very little affected by the gap variations of the window layer.

The efficiency (E_{ff}) variations as a function of E_g of the window layer are also illustrated in Fig. 2d. It is clear that the efficiency has a better value for a window layer band gap ranging from 2.05 eV to 2.10 eV. Beyond 2.10 eV, the value of the efficiency starts to decrease with increasing E_g of the window layer.

To better understand the reasons for improving the cell efficiency as a function of E_g of the window layer for values ranging from 2.05 to 2.10 eV, we have plotted the energy band diagrams in Fig. 4. From the latter, we calculated and grouped in Table 2 the values of the band diagram discontinuities on the conduction band levels ΔE_{C1} and ΔE_{C2} and on the valence band levels ΔE_{V1} (interface between the window layer and the buffer layer) and ΔE_{V2} (interface between the buffer layer and the active layer).

From Table 2 it is clear that the values of ΔE_{C1} and ΔE_{C2} are invariable and they serve as beneficial mirrors for the reflection of the electrons that move towards the front contact. However, ΔE_{V2} (interface between the buffer layer and the active layer) has a low value and invariable. On the other hand, ΔE_{V1} (interface between the window layer and the buffer layer) is variable, depends on the window layer band gap (E_g) and takes a very low value of 0.02 eV for an E_g equal to 2.05 eV, snce ΔE_{V1} and ΔE_{V2} are barriers for holes which move towards the front contact. However, these low values promote and facilitate the collection of photogenerated holes at the front contact; this explains why the efficiency of the cell is better for Eg equal to 2.05 eV.

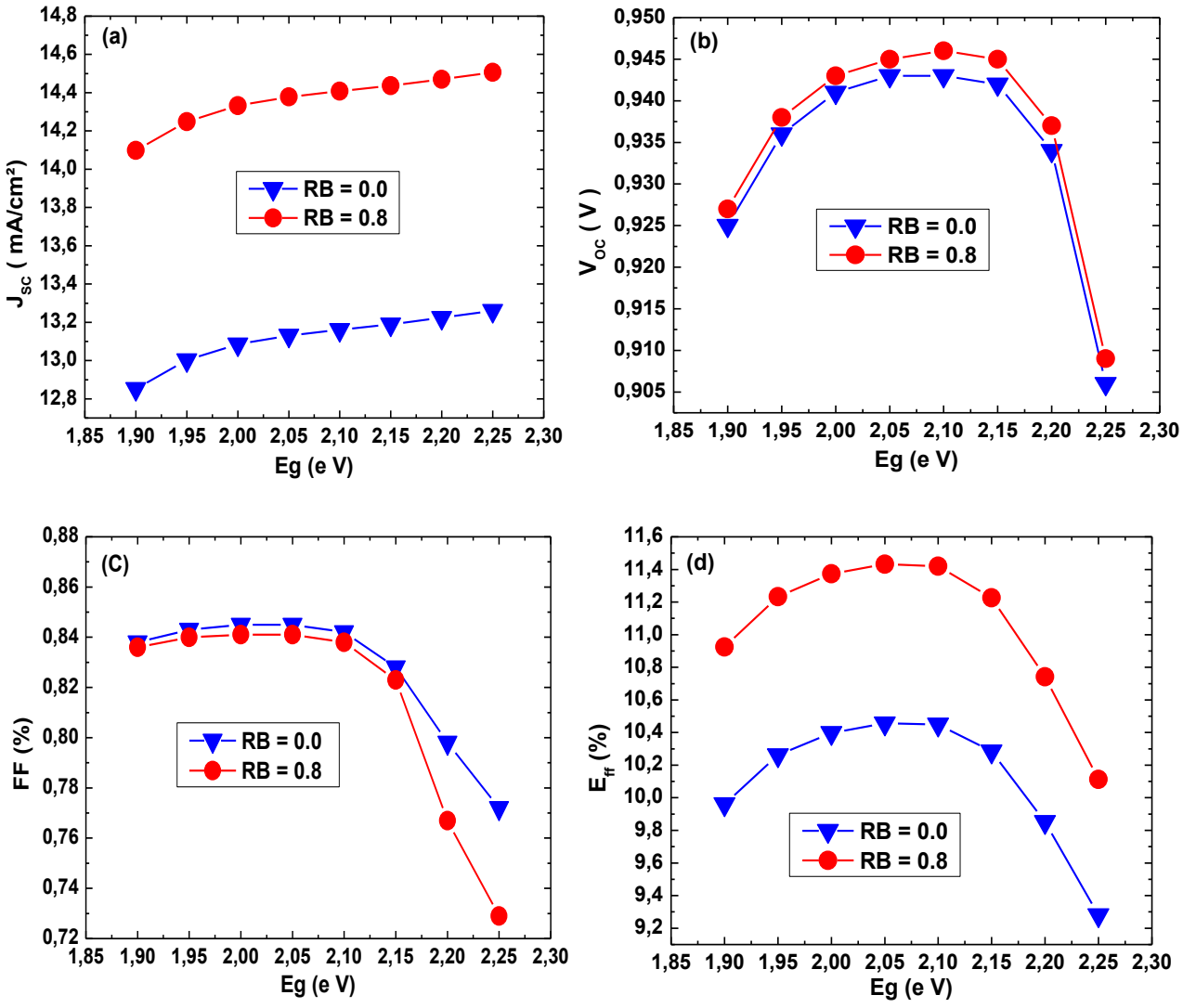

Fig. 2 – Variations of the J_{SC} (a), V_{OC} (b), *FF* (c) and efficiency with *p-nc*-SiO*x*:H window layer band gap (E_g) (d)

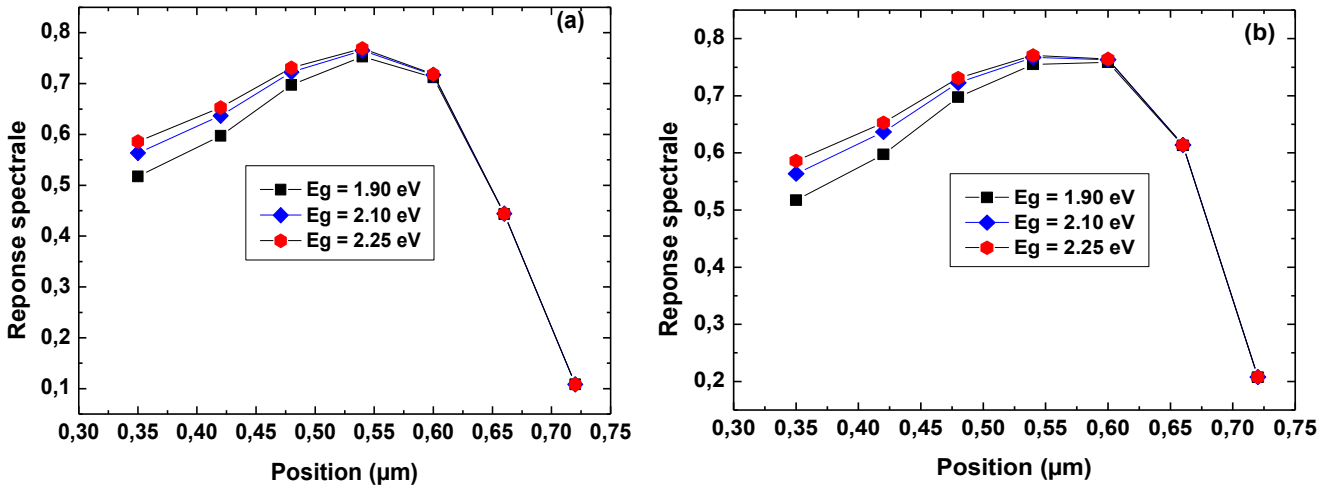

Fig. 3 – External quantum efficiency for the simulated structure for two values of the back reflection RB = 0 (a) and RB = 0.8 (b)

The abbreviations used in this Table are the following: ε_r is the relative dielectric permittivity, L is the film thickness, χ is the electron affinity, E_g is the energy band gap, μ_e, μ_h are the mobilities of electrons and holes; N_D, N_A are the doping donors and acceptors; N_C, N_V are the effective densities of states in the conduction and valence bands; N_{DG}, N_{AG} are the Gaussian

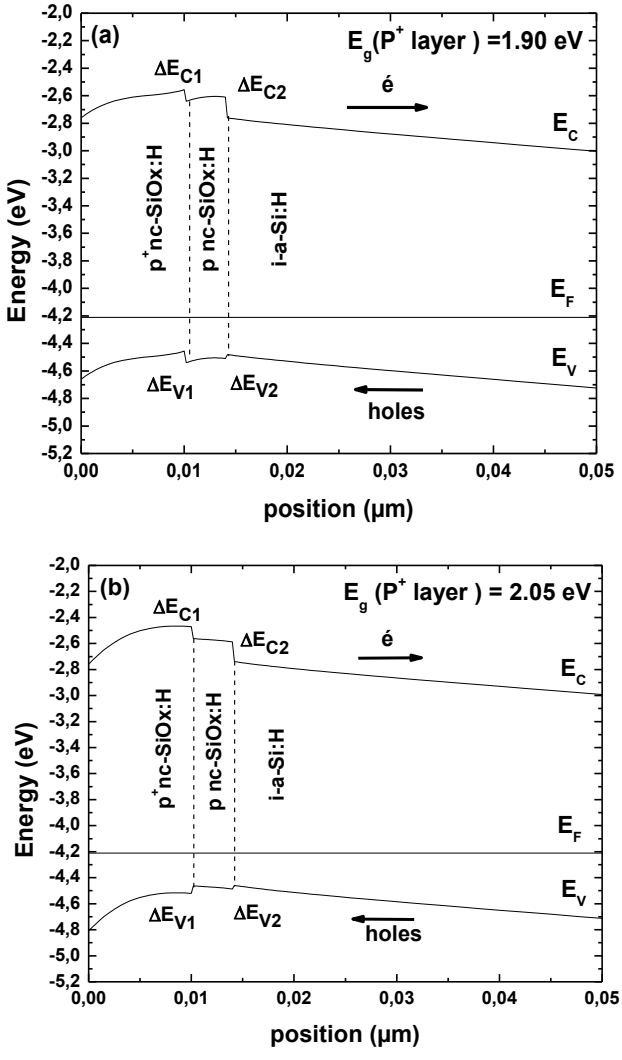

densities for donor and acceptor states; G_{DO}, G_{AO} are the exponential pre-factors of donor-like and acceptor-like tail states; E_D, E_A are the characteristic energy of the donor-like/acceptor-like tail states [14-16].

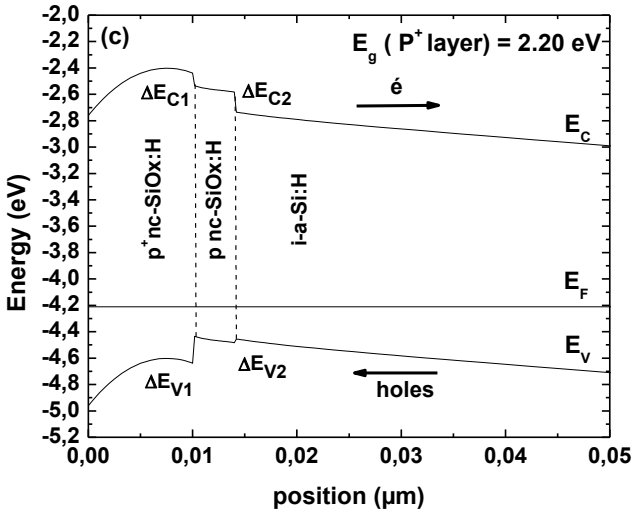

Fig. 4 – Energy band diagram of the simulated solar cells when the *p-nc*-SiO*x*:H window layer band gap is E_g = 1.9 eV (a), E_g = 2.05 eV (b), E_g = 2.20 eV (c)

Table 1 – Material parameters used for AMPS-1D simulations at room temperature

Parameters	*p nc*-SiO*x*:H	*p nc*-SiO*x*:H	*i*-a-Si: H	*n*-a-Si:H
ε_r	11.9	11.9	11.9	11.9
L (nm)	10	05	300	25
X (eV)	3.76	3.78	3.80	3.80
E_g (eV)	Variable	2.05	1.72	1.72
N_C (cm^{-3})	10^{23}	10^{23}	$2.5\cdot10^{20}$	$2.5\cdot10^{20}$
N_V (cm^{-3})	10^{23}	10^{23}	$2.5\cdot10^{20}$	$2.5\cdot10^{20}$
μ_e (cm^{2}V^{-1}S^{-1})	5	7	20	10
μ_h (cm^{2}V^{-1}S^{-1})	0.5	0.7	2	1
N_A (cm^{-3})	$2\cdot10^{19}$	5×10^{18}	0	0
N_D (cm^{-3})	0	0	0	10^{19}
G_{DO}/G_{AO}(cm^{-3}eV^{-3})	10^{22}	10^{22}	$2\cdot10^{21}$	$2\cdot10^{21}$
E_D/E_A (eV)	0.06/0.03	0.05/0.02	0.04/0.02	0.05/0.03

Table 2 – Band discontinuities extracted from the energy and diagram of the simulated structure at thermodynamic equilibrium

E_g (eV), window layer	ΔE_{C1}, (eV)	ΔE_{C2}, (eV)	ΔE_{V1}, (eV)	ΔE_{V2}, (eV)
1.90	0.1	0.17	0.1	0.01
2.05	0.1	0.17	0.02	0.01
2.20	0.1	0.18	0.2	0.01

4. CONCLUSIONS

The study carried out in this work was conducted on two solar cells of substrate type (*n-i-p*), one without a rear reflector (RB = 0) and the other with a rear reflector (RB = 0.8). For this, we have used the AMPS-1D code to investigate by numerical simulation the simultaneous effect of the *p*-window layer (based on hydrogenated nanocrystalline silicon oxide) band gap (E_g), and the presence of a rear reflector, in the structure, on the solar cell performances. The simulation results showed that the best output parameters, like the short-circuit current (J_{SC}), the open-circuit voltage (V_{OC}), and the efficiency (E_{ff}) can be improved with the presence of a rear reflector (RB = 0.8). It is obtained that the efficiency improvement is due essentially to the short-circuit current improvement. However, the value of the conversion efficiency was improved from 10.45 % (structure without a rear reflector) to 11.43 % (structure with a rear reflector), when the Jsc value was improved from 13.16 mA/cm² (for RB = 0) to 14.40 mA/cm² (for RB = 0.8). The latter best values of J_{SC} and efficiency were obtained when the p-window layer band gap was equal to 2.05 eV.

ACKNOWLEDGEMENTS

The authors are grateful to Prof. S. Fonash from the Pennsylvania State University for providing the AMPS-1D program used in this work.

REFERENCES

1. D. Carlson, C. Wronski, *Appl. Phys. Lett.* **28**, 671 (1976).
2. J. Yang, A. Banerjee, S. Guha, *Appl. Phys. Lett.* **70**, 2975 (1997).
3. M. Kondo, *Sol. Energ. Mater. Sol. C.* **78**, 543 (2003).
4. A. Klaver, R.A.C.M.M. van Swaaij, *Sol. Energ. Mater. Sol. C.* **92**, 50 (2008).
5. E.A. Schiff, *J. Phys: Condens. Matter* **16**, S5265 (2004).
6. B. Yan, J. Yang, S. Guha, *J. Vac. Sci. Technol. A* **30**, 04D108 (2012).
7. B. Yan, G. Yue, J. Yang, S. Guha, *Sol. Energ. Mater. Sol. C.* **111**, 90 (2013).
8. J. Meier, J. Spitznagel, U. Kroll, C. Bucher, S. Faÿ, T. Moriarty, A. Shah, *Thin Solid Films* **451-452**, 518 (2004).
9. F. Finger, Y. Mai, S. Klein, R. Carius, *Thin Solid Films* **516**, 728 (2008).
10. P. Buehlmann, J. Bailat, D. Dominé, A. Billet, F. Meillaud, A. Feltrin, C. Ballif, *Appl. Phys. Lett.* **91**, 143505 (2007).
11. P.J. McElheny, J.K. Arch, H.-S. Lin, S.J. Fonash, *J. Appl. Phys.* **64**, 1254 (1988).
12. Y. Mai, S. Klein, R. Carius, H. Stiebig, X. Geng, F. Finger, *Appl. Phys. Lett.* **87**, 073503 (2005).
13. S. Fonash, J. Arch, J. Hou, W. Howland, P. Mcelheny, A. Moquin, M. Rogosky, T. Tran, H. Zhu, F. Rubinelli, *A manual for AMPS-1D for windows 95/NT a One-Dimensional Device Simulation Program for the Analysis of Microelectronic and Photonic Structures*. (The Pennsylvania State University: 1997).
14. A. Belfar, B. Amiri, H. Ait-Kaci, *J. Nano- Electron. Phys.* **7** No 2, 02007 (2015).
15. A. Belfar, *Optik* **126**, 5688 (2015).
16. A. Belfar, H. Ait-Kaci, *Thin Solid Films* **525**, 167 (2012).

Одночасний вплив ширини забороненої зони віконного шару *p-nc*-SiO*x*:H та зворотного відбиття на характеристики сонячних елементів на основі a-Si:H

Abbas Belfar, Mohammed Belmekki, Ferroudja Hammour, Hocine Ait-Kaci

Laboratory of Plasma Physics, Conductor Materials and their Applications, Faculty of Physics, Oran University of Sciences and Technology Mohamed Boudiaf USTO-MB, BP1505 Oran, Algeria

У роботі представлені результати чисельного моделювання одночасного впливу ширини забороненої зони віконного шару *p-nc*-SiO*x*:H (E_g) і зворотного відбиття (RB) на фотогальванічні характеристики сонячних елементів з гідрогенізованого аморфного кремнію (a-Si:H). Для моделювання ми використали код AMPS-1D (одномірний аналіз мікроелектронних і фотонних структур). Моделювання проводилося на двох конфігураціях досліджуваного елементу, одна без заднього відбивача (RB = 0), а інша із заднім відбивачем (RB = 0.8). Результати моделювання показали, що найкращі вихідні параметри елементу були отримані у випадку структури з заднім відбивачем і коли значення ширини забороненої зони *p*-вікна лежить в діапазоні від 2.05 еВ до 2.10 еВ. З одного боку, значення розривів на зонній діаграмі рівнів зони провідності ΔE_{C1} and ΔE_{C2} і рівнів валентної зони ΔE_{V1} (межа поділу між віконним шаром і буферним шаром) і ΔE_{V2} (межа поділу між буферним шаром і активним шаром) досліджені для кращого розуміння варіацій ефективності (E_{ff}) як функції E_g віконного шару. З іншого боку, отримано, що спектральна характеристика (SR) дуже чутлива до коливань ширини забороненої зони віконного шару в діапазоні довжин хвиль від 0.35 до 0.55 мкм для обох випадків. Проте спектральна характеристика зменшується зі збільшенням E_g. Нарешті, спектральна характеристика сонячних елементів покращилася в діапазоні довжин хвиль від 0.55 до 0.7 мкм, а найкраще значення ефективності E_{ff} = 11.43 % було отримано у випадку структури з заднім відбивачем.

Ключові слова: Сонячний елемент, Гідрогенізований нанокристалічний оксид кремнію, Зворотне відбиття, Заборонена зона віконного шару.